Janus hollow fibre membranes with intrusion anchored structure for robust desalination and leachate treatment in direct contact membrane distillation

This is the Published version of the following publication

Yang, Guang, Ng, Derrick, Huang, Zhen, Zhang, Jianhua, Gray, Stephen and Xie, Zongli (2023) Janus hollow fibre membranes with intrusion anchored structure for robust desalination and leachate treatment in direct contact membrane distillation. Desalination, 551. ISSN 0011-9164
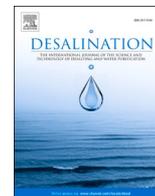
Janus hollow fibre membranes with intrusion anchored structure for robust desalination and leachate treatment in direct contact membrane distillation

Guang Yang [a,b,c], Derrick Ng [a], Zhen Huang [a,b], Jianhua Zhang [b], Stephen Gray [b], Zongli Xie [a,*]

[a] *CSIRO Manufacturing, Private Bag 10, Clayton South, Vic. 3169, Australia*
[b] *Institute for Sustainable Industries and Liveable Cities, Victoria University, PO Box 14428, Melbourne, Vic. 8001, Australia*
[c] *School of Environmental and Chemical Engineering, Shenyang Ligong University, Liaoning 110159, China*

HIGHLIGHTS

- An intrusion-anchored layer was formed on hydrophobic hollow fibre membrane.
- The active layer can be tuned from 2-D laminar stacks to 3-D mixed matrix hybrids.
- The GO nanosheets formed covalent linkages with PVA and SSA.
- The fabricated membrane was applied to seawater and leachate wastewater treatment.

ABSTRACT

High-performance Janus membranes have been intriguing for membrane distillation due to its distinctive features for improving fouling and wetting resistance. However, long-term structural stability remains challenging owing to delamination caused by the opposite affinity between the two different kinds of materials. Herein, a physically-anchored hydrophilic layer containing graphene oxide (GO)/poly(vinyl alcohol) (PVA)/sulfosuccinic acid (SSA) i.e., GOSP layer was formed on the surface of a microporous polypropylene (PP) hollow fibre membrane. Meanwhile, the nanostructure of the GOSP layer could be tuned from 2-dimensional lamellar to 3-dimensional mixed matrix, exhibiting various water transport properties. As a result, the fabricated Janus membrane with the partially intruded pore channels exhibited superior antiwetting and antifouling performance for desalination and wastewater treatment in the direct contact membrane distillation process. For surfactant containing saline water, the GOSP/PP Janus membrane with optimised PVA/GO ratio possessed noticeably enhanced anti-wetting property compared to pristine PP membrane. In particular for leachate treatment, the GOSP/PP membrane produced high quality permeate with <1 mg/L ions and 10 mg/L total organics and maintained stable water flux while the leachate was concentrated by 5 times (80 % water recovery), providing great potential for using membrane distillation towards zero liquid discharge.

1. Introduction

Water scarcity is one of the top global challenges to meet the high demand of ever-growing population and industries. It is well recognised that seawater desalination or the reclamation of water from wastewaters can provide alternative water resources to enhance environmental sustainability and resilience. However, since industrial wastewater or brine concentrate often processes a complex chemical composition and high salinity, challenges such as high-pressure requirement, secondary pollution, high fouling tendency and short membrane lifetime, limit the application of current reverse osmosis membrane desalination technology [1–3]. A treatment option that is able to withstand the impacts of high salt concentration and fouling is sought.

Membrane distillation (MD), an emerging desalination technology, is a thermally-driven separation process associated with the transport of water vapor through microporous hydrophobic membranes [4,5]. The driving force for separation is a vapor pressure gradient caused by a temperature difference across the MD membrane [6]. MD well suits recovering water from hypersaline water where low-grade waste heat can be utilized. However, since the chemical composition of the targeted

feed solution is usually complex and accompanied with low surface tension property due to the existence of organics and surfactants, the hydrophobic membranes are prone to wetting and fouling during the MD operation, leading to water vapor flux decline and deterioration of the product quality [7–9]. To date, extensive studies have been conducted to improve the resistance of MD membranes to wetting and fouling by various methods including hydrophobic modification, hydrophilic modification, oleophobic modification and omniphobic modification [10–14]. Among these methods, hydrophilic modification of the MD membrane to form a Janus membrane has been attractive since a hydrophilic membrane surface containing polar or charged groups has less tendency to fouling than the hydrophobic surface [15–18]. In addition, the hydrophilic surface repels the hydrophobic moieties of the wetting resistance of the MD membrane [16]. Currently, the state-of-the-art Janus membranes for antiwetting and antifouling MD are designed by integrating hydrophilic polymers and functional nanomaterials on hydrophobic or omniphobic substrates [19]. Huang et al. prepared hydrophilic multilayers on electrospun fibrous cetyltrimethylammonium bromide/poly(vinylidene fluoride-*co*-hexafluoropropylene) (CTAB/PVDF-HFP) substrate using fluorinated silica nanoparticles (SiNPs) to form the first layer and polymer composite consisting SiNPs, chitosan and perfluorooctanoate as the second layer [20]. The fabricated membranes exhibited outstanding antiwetting performance towards the feeds with increasing concentrations of sodium dodecyl sulfate (SDS) (from 0.1 mM to 0.4 mM) while the control hydrophobic PVDF-HFP membrane was wetted in the presence of SDS, showing increased water fluxes by multiple times and decreased salt rejection down to 40 %. On the other hand, the Janus membrane also exhibited stable salt rejection and water fluxed when processing oil-in-water emulsion. As a comparison, the PVDF-HFP membrane was fouled when the MD was conducted within only 1 h by decreasing the flux decreased to <20 % of the initial flux. Commercial PVDF hollow fibre membranes were modified via dopamine polymerization on the surface followed by in situ immobilization of silver nanoparticles (AgNPs) [21]. The resultant Janus membranes with multilevel surface roughness exhibited robust long-term stability in surfactant solutions as well as emulsions in a 96-h bench-scale test whereas a rapid decrease in salt rejection with fast fluctuation in water fluxes was observed for the PVDF membrane. It was demonstrated that thin poly(vinyl alcohol) (PVA)/metal-organic framework (MOF) mixed matrix membrane could be used as the hydrophilic layer to enhance the antiwetting and stability of the fabricated Janus membrane when the dispersion of the MOF particles was uniform [15]. However, the agglomeration of the MOF particles gave rise to decline of the separation performance. As for the Janus membranes for MD, it is challenging to obtain good interfacial attachment owing to the immiscibility between the two layers [22,23]. Hydrophilic modification with low mass transport resistance and high structural stability is therefore highly desired for practical and energy-efficient MD applications [24,25].

In recent years, laminar assembly of graphene oxide (GO) nanosheets has been appealing as a novel platform for molecule separations due to its frictionless two-dimensional (2D) nanochannels and precise molecular sieving property [26–29]. Owing to the existence of polar functional groups, the hydrophilic property of the GO nanosheets makes them particularly attractive as the modifier for MD membranes. For example, Bhadra et al. [30] immobilized GO nanosheets on polytetrafluoroethylene (PTFE) membrane surface and used the GO immobilized membrane (GOIM) for desalination via direct contact MD (DCMD). For the GOIM membrane, the water flux (94 kg/m^2 h at 80 °C feed temperature and 20 °C at permeate side) was 35 % higher than the pristine membrane and that could be attributed to the GO-introduced features including selective sorption, nanocapillary effect, reduced temperature polarization as well as the presence of polar functional groups. However, a significant challenge for the application of the GO laminar assembles in aqueous environment is the water-induced swelling (enlargement of the interlayer spacing) [31,32]. Our previous study demonstrated the

crosslinking of GO nanosheets using hydrophilic chemicals with dual reactive entities is an efficient strategy to enhance the swelling resistance while increasing the water transport in a pervaporation process [33]. As such, employing crosslinked GO is promising for the hydrophilic modification of MD membranes to enhance the antiwetting and fouling capability of MD membranes.

Herein, the hydrophilic modification of a polypropylene (PP) hollow fibre MD membrane using GO as a building block and sulfosuccinic acid (SSA) as a crosslinker is presented. PVA was employed as a flexible spacer as well as a reactive bridging agent for the crosslinked GO assemblies, rendering both increased hydrophilicity and tunable permeability of the GO network. In this work, the PVA to GO ratio varied from 0.1 to 10, giving rise to a variation from 2D laminar structure to three-dimensional (3D) mixed matrix structure. The MD performances related to the aforementioned structures were compared for the first time. In addition, the pores of the modified PP based MD membrane were partially intruded by the PVA/GO/SSA mixed material, leading to an anchored Janus construction and thus a Janus pore channel. Then, the resultant membrane was applied in DCMD process towards real seawater desalination and leachate treatment where the results demonstrated that attaching the GO/PVA/SSA hydrophilic layer on the PP substrate effectively enhanced the antiwetting property and stability as compared with the bare PP membrane. This work provided a feasible strategy of hydrophilic modification of MD membranes for potential application in wastewater treatment towards zero liquid discharge and in-depth understanding of the structure-performance relationship for antiwetting and antifouling MD.

Nomenclature

GO	graphene oxide
PVA	poly (vinyl alcohol)
SSA	sulfosuccinic acid
GOSP	graphene oxide/poly (vinyl alcohol)/sulfosuccinic acid
PP	polypropylene
MD	membrane distillation
DCMD	direct contact membrane distillation
CTAB	cetyltrimethylammonium bromide
PVDF-HFP	poly(vinylidene fluoride-co-hexafluoropropylene)
SiNPs	silica nanoparticles
SDS	sodium dodecyl sulfate
PVDF	polyvinylidene fluoride
AgNPs	silver nanoparticles
MOF	metal-organic framework
2D	two-dimensional
3D	three-dimensional
PTFE	polytetrafluoroethylene
GOIM	graphene oxide immobilized membrane
NaCl	sodium chloride
HF	hollow fibre
EC	electrical conductivity
GOSP/PP-0.1	graphene oxide/poly (vinyl alcohol)/sulfosuccinic acid on polypropylene with 10 wt% poly(vinyl alcohol) and 20 wt% sulfosuccinic acid in weight percentages to graphene oxide
GOSP/PP-1	graphene oxide/poly (vinyl alcohol)/sulfosuccinic acid on polypropylene with 100 wt% poly(vinyl alcohol) and 20 wt% sulfosuccinic acid in weight percentages to graphene oxide
GOSP/PP-10	graphene oxide/poly (vinyl alcohol)/sulfosuccinic acid on polypropylene with 1000 wt% poly(vinyl alcohol) and 20 wt% sulfosuccinic acid in weight percentages to graphene oxide
GOSP/PP-0.1(10)	graphene oxide/poly (vinyl alcohol)/sulfosuccinic acid on polypropylene with 10 wt% poly(vinyl alcohol) and 20 wt% sulfosuccinic acid in weight percentages to graphene oxide; the concentration of the graphene oxide stock solution is 0.1 mg/L

GOSP/PP-0.1(50)   graphene oxide/poly (vinyl alcohol)/sulfosuccinic acid on polypropylene with 10 wt% poly(vinyl alcohol) and 20 wt% sulfosuccinic acid in weight percentages to graphene oxide; the concentration of the graphene oxide stock solution is 0.5 mg/L

GOSP/PP-0.1(100)   graphene oxide/poly (vinyl alcohol)/sulfosuccinic acid on polypropylene with 10 wt% poly(vinyl alcohol) and 20 wt% sulfosuccinic acid in weight percentages to graphene oxide; the concentration of the graphene oxide stock solution is 1 mg/L

FESEM	field emission scanning electron microscope
WCAs	water contact angles
ATR-FTIR	attenuated total reflectance-Fourier transform infrared
DSC	differential scanning calorimetry
ICP-OES	inductively coupled plasma optical emission spectroscopy
LEP	liquid entry pressure
XRD	X-ray diffraction
J	water flux (kg/m^2 h)
ΔW	mass change of permeate (kg)
A	effective membrane area (m^2)
t	time interval during the permeate mass change (h)
Jn	normalized flux (kg/m^2 h)
Jm	water flux obtained for the required test (kg/m^2 h)
J_0	water flux when the feed was DI water (kg/m^2 h)
W_R	water recovery (%)
V_0	initial feed volume (L)
Vt	volume of feed at time t (h)
V_p	volume of the permeate (L)
R	salt rejection (%)
Cp	salt concentration in the permeate (mg/L)
Cf	salt concentration in the feed (mg/L)

2. Experimental

2.1. Materials

PVA (Mw = 96,000 g/mol), absolute ethanol, SSA (70 wt%), sodium chloride (NaCl), SDS and mineral oil (heavy grade) were all sourced from Sigma-Aldrich. GO nanosheets (length 0.5–5 μm, thickness 0.8–1.2 nm) were purchased from XFNano Inc., China. All chemicals were analytical grade and used as received. Commercial PP hollow fibre membranes with pore size in the range of 0.3–0.8 μm were bought from Membrana GmbH, Germany. The seawater was collected from Black Rock Beach in Melbourne, Australia. The main cation concentrations of the real seawater are listed in Table S1 in the Supplementary Information (SI). The landfill leachate was obtained from Environmental Group Ltd. (EGL), Australia.

2.2. Synthesis of Janus membranes

To prepare PVA stock solution, 6 g of PVA was added into 94 g of DI water whilst stirring, the solution was then heated to 95 °C under stirring for 4 h. To prepare GO stock solution, 50 mg of GO was added into 100 mL DI water, followed by sonication in an ice bath for 3 h. A series of coating solutions were then made by mixing the required amount of PVA stock solution, SSA and GO solution, where the SSA was fixed at 20 wt% with respect to GO and the concentration of PVA relative to GO was varied, namely 10, 100 and 1000 wt%. The corresponding membranes were then named GOSP/PP-0.1, GOSP/PP-1 and GOSP/PP-10 respectively. Another series was made by specifically fixing the optimum PVA to GO ratio at 10 wt% but changing GO amounts to 10, 50 and 100 mg in the GO stock solution, and the resulting membrane samples were named GOSP/PP-0.1(10), GOSP/PP-0.1(50), GOSP/PP-0.1(100), respectively. The specific compositions of the aforementioned hydrophilic layers were listed in Table 1.

Hollow fibre (HF) membrane modules were assembled via an epoxy-

Table 1
Compositions of the hydrophilic layers.[a]

Membranes	GO loading (wt %)	PVA loading (wt %)	SSA loading (wt %)
GOSP/PP-0.1	76.9	7.7	15.4
GOSP/PP-1	45.5	45.5	9.0
GOSP/PP-10	8.9	89.3	1.8
GOSP/PP-0.1(10)	76.9	7.7	15.4
GOSP/PP-0.1(50)	76.9	7.7	15.4
GOSP/PP-0.1 (100)	76.9	7.7	15.4

[a] GOSP/PP-0.1(10), GOSP/PP-0.1(50) and GOSP/PP-0.1(100) refer to the samples in which the PVA to GO ratio was fixed and the GO concentrations in the stock solutions were 0.1, 0.5 and 1 mg/L, respectively.

potting technique [34,35] containing 20 fibres with the effective length of the membrane of 200 mm (shown in Fig.S1 in the SI). The preparation of the Janus membrane was realized by an ethanol-assisted vacuum filtration process. Briefly, ethanol was first introduced unto the shell side of the membrane modules and the membranes soaked in the ethanol for 30 s in order to wet the outer surface of the HFs. Then, the above-mentioned coating solution prepared was added unto the shell side of module, and vacuum filtered through the PP HF surface until no permeate was observed. The coated module was then gently blow-dried using air in both the lumen and shell sides and then thermally treated in an oven at 75 °C for 2 h.

2.3. Membrane testing

Fig. 1 shows a schematic drawing of the lab scale DCMD testing system employing hollow fibre membrane module. The feed solution (1 L) was first heated to 50 °C via a water bath, and then pumped into the shell side of the HF module; DI water (500 mL) was cooled to 10 °C and circulated at the lumen side of the membrane. Two peristaltic pumps were used to circulate flows in a counter-current mode both at flowrates of 350 mL/min. The mass of the cold permeate water were weighted using a digital scale (A&D, Model GF-6000) equipped with a data acquisition system. The electrical conductivity (EC) of the permeate stream was monitored continuously with a conductivity meter (Hanna HI98192) to evaluate salt rejection and anti-wetting property of the GOSP/PP membranes. The water flux (J) was calculated by the following equation [36]:

$$J = \frac{\Delta W}{At} \tag{1}$$

where J is the permeate flux, ΔW is the mass change of permeate (kg), A is the effective membrane area (m^2) and t represents the time interval (hour) during the permeate mass change. For better comparison, the normalized flux (J_n) was utilized and calculated using the J_m as obtained for the required test and J_0 when the feed was DI water:

$$J_n = \frac{J_m}{J_0} \tag{2}$$

For each experiment, water recovery (W_R) is obtained by Eq. (3), where V_0 (L) and V_t (L) are the initial feed volume and volume of feed at time t (h);

$$W_R = \left(1 - \frac{V_t}{V_0}\right) \times 100\% \tag{3}$$

The salt rejection (%) was determined by Eq. (4) as described elsewhere [37,38]:

$$R = \left(1 - \frac{V_p C_p}{JAtC_f}\right) \times 100\% \tag{4}$$

C_p and C_f are denoted as the salt concentration in the feed and permeate solutions, respectively. V_p was the volume of the permeate.
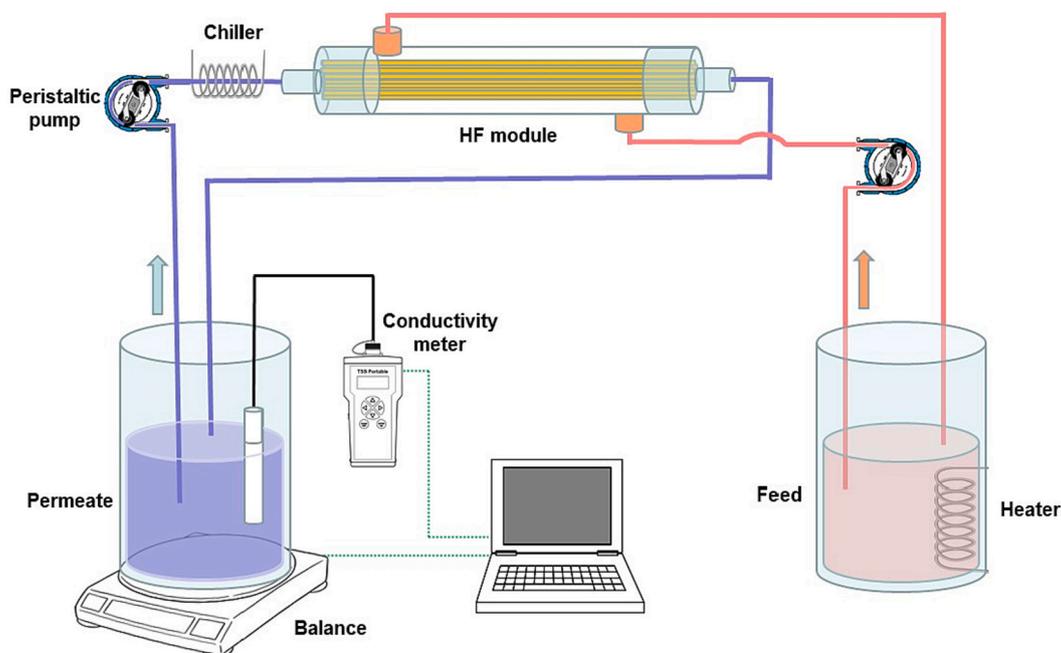
Fig. 1. Schematic of experimental set up for HF membranes in a DCMD process.

2.4. Characterization

Surface and cross-sectional morphologies of the membranes were examined by a field emission scanning electron microscope (FESEM, Zeiss Merlin Gemini2). Surface roughness was analysed by a 3D laser microscope (Olympus OLS4100 LEXT). The water contact angles (WCAs) were measured by an optical tensiometer (KSV CAM200) to ascertain the hydrophobicity or hydrophilicity of the membranes. Both the inner and outer surface of the membranes were measured via slicing open the HFs followed by flattening on the sample plate. The chemical structure was evaluated by attenuated total reflectance-Fourier transform infrared (ATR-FTIR) spectroscopy (Perkin-Elmer Spectrum 2000 FTIR instrument) for both the GO and HF membranes. The crystalline structures of the GO and membranes were studied using X-ray diffractometer (Rigaku SmartLab X-ray diffractometer). Inductively coupled plasma optical emission spectroscopy (ICP-OES) analysis was conducted using Varian 730 ICP-OES after the as-prepared membrane samples was immersed in water for 48 h and acidified with nitric acid for elemental detection. Liquid entry pressure (LEP) of membranes were measured according to the method as described by the literature [39,40], the

modified experimental set up is illustrated in Fig. 2. A high-pressure stainless-steel vessel was filled with DI water and subjected to air pressure adjusted by a regulator. The downstream of the vessel was then connected to a shell side of a dry HF module, the other end of the shell side and one end of the lumen side were capped off. Pressure was increased slowly with an increment of 0.5 kPa whilst monitoring the digital pressure transducer. The pressure at which DI water started to flow from the uncapped lumen side is taken as the LEP value of the HF membrane.

3. Results and discussion

3.1. Physicochemical property of the GOSP layer

As shown in Fig. 3, the ATR-FTIR spectrum of the GO nanosheets shows adsorption bands at 1089 cm^{-1}, 1250 cm^{-1}, 1644 cm^{-1}, 1731 cm^{-1} and 3390 cm^{-1}, which can be attributed to the functional groups of C-O-C, C—O, C—C, C=O and -OH, respectively [41]. For the PVA, it can be identified by the characteristic bands ranging from 3000 to 3700 cm^{-1} for the hydrogen bonded -OH groups and peaks at 2985 and 2820
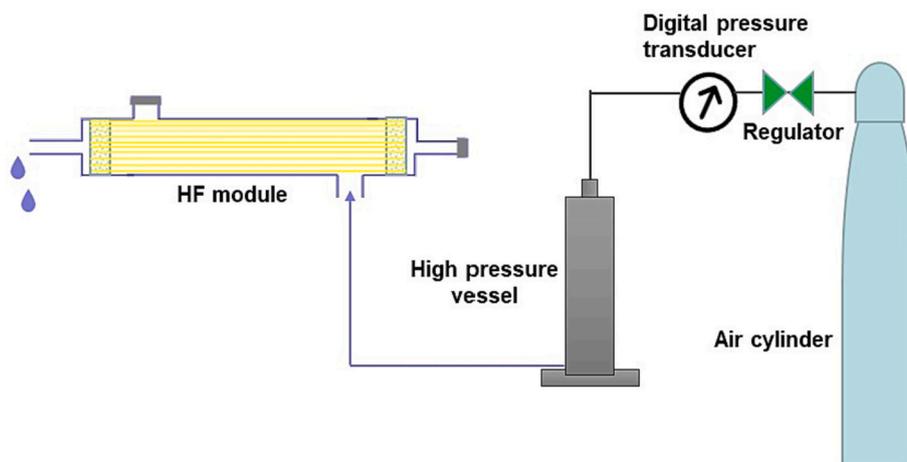
Fig. 2. Schematic of experimental set up for LEP measurements.
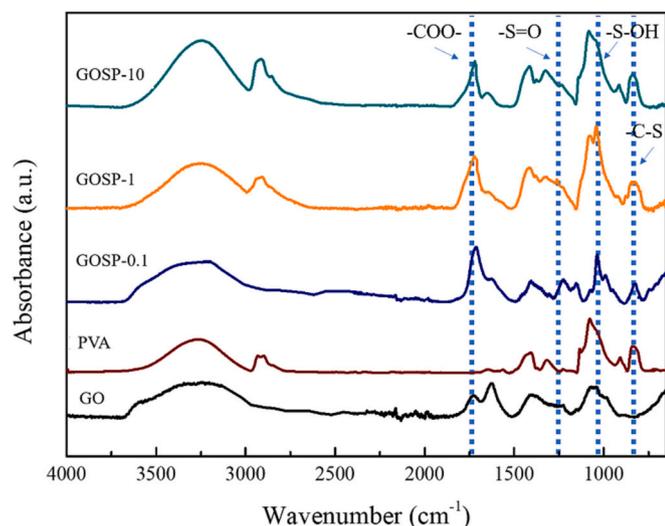
Fig. 3. ATR-FTIR spectrum of the free-standing films.

cm^{-1} for the asymmetric and symmetric stretching of -CH groups, respectively, 1450 cm^{-1} for CH$_2$ (from the PVA backbone) bending vibration and 1085 cm^{-1} for C—O of the hydroxyl groups [42]. After the addition of SSA and PVA into the GO, the GOSP/PP-1 exhibited new peaks at 725, 1048, 1184 and 1725 cm^{-1} which corresponded to the stretching vibration of C—S, S–OH, S=O and -COO-. This indicated that the SSA was covalently linked to the GO nanosheets via the formation of ester groups while retaining its sulfonic acid groups. When the content of PVA was increased from 0.1 to 10, the peak intensity of -COO- was also increased accordingly, suggesting that the intercalated PVA molecules were also forming ester groups either with SSA or GO. In order to further investigate the formation of the covalent linkage between them, freestanding GO/PVA, GO/SSA and PVA/SSA films were prepared and the FTIR spectra are shown in Fig.S2 in the SI. It can be seen that the characteristic peaks of ester groups were hardly observed in GO/PVA while GO/SSA and PVA/SSA formed the ester groups (-COO-) by

exhibiting adsorption peaks at 1725 cm^{-1}. This could be attributed to the SSA releasing hydrogen ions when dissolved in water. As a result, the hydrogen ions alter the pH of the solution as required for the esterification reaction. In addition, it was reported that sulfonic acid groups also act as catalysts for condensation and esterification reactions [43,44]. Therefore, the SSA dominated the covalent linkage within the membrane.

The GO nanosheets and GOSP layers were analysed by X-ray diffraction (XRD) patterns to compare the d-spacing change in both dry and wet state. As shown in Fig. 4, the dry GO exhibited a characteristic peak at 11.08°, corresponding to a d-spacing of 0.80 nm. For the GOSP-0.1 and GOSP-1, the d-spacing increased to 0.89 nm (9.84°) for GOSP-0.1 and 1.39 nm (6.34°) for GOSP/PP-1, respectively. However, the GOSP-10 film mainly exhibited the orthorhombic lattice (101) of PVA (19.5°). This indicated that the nanoscale structure of the GOSP film was altered from the 2D laminate to the mixed matrix hybrid when the PVA content in GOSP was high (10 times higher than the GO as in GOSP-10), leading to the disorder of GO alignments and thus the random distribution in the PVA matrix. On the other hand, the GO and GOSP layer showed different swelling characteristic in the wet state after the samples were immersed in DI water for 12 h and wiped off the water on the surfaces. As can be seen in Fig. 4, the characteristic peak of GO shifted down to 6.81° in the wet state, corresponding to a significant increased d-spacing of 1.29 nm as opposed to 0.80 nm at the dry state, indicating significant swelling of GO as expected. In contrast, the XRD pattern of the GOSP/PP-0.1 and GOSP/PP-1 demonstrated the d-spacing of 1.24 and 1.86 nm, respectively. The XRD pattern for wetted GOSP/PP-10 remained relatively stable compared with the dry state since PVA was semi-crystalline polymer. In summary, the GO exhibited a 63 % increase in the d-spacing while the GOSP/PP-0.1 and GOSP/PP-1 exhibited only 39 % and 34 % increases, respectively. These results demonstrated that the covalent linkage among GO, SSA and PVA played a critical role in restraining the swelling of GO nanosheets.

3.2. Morphology of the Janus membranes

3D laser microscope was utilized for imaging the outer surface of the
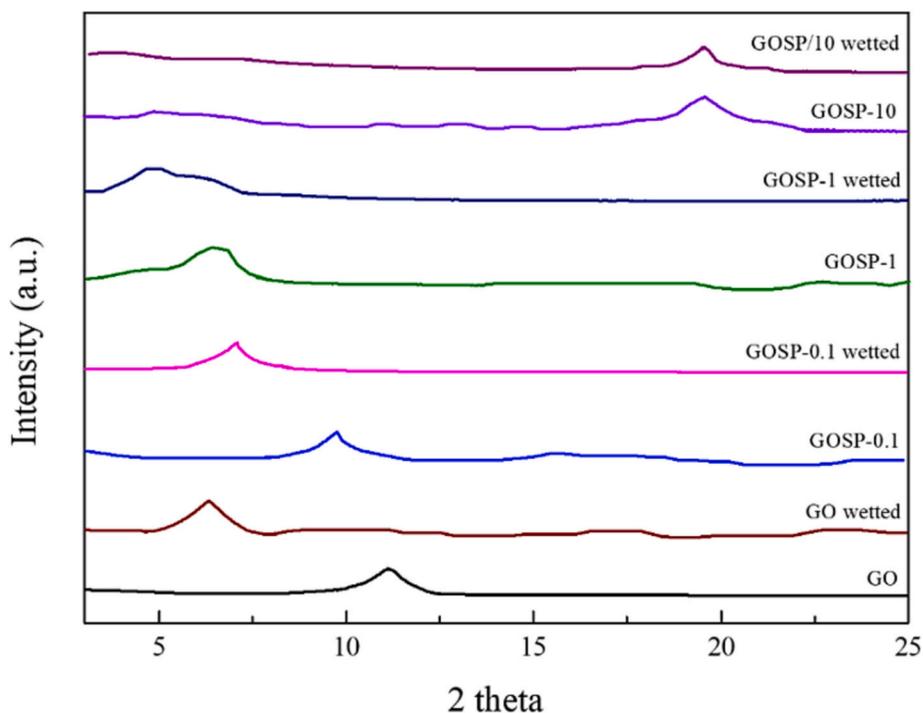
Fig. 4. XRD results of the synthesized membrane materials.

PP and GOSP/PP hollow fibre membranes as shown in Fig. 5. Compared to the PP, the GOSP/PP exhibited similar surface morphology, but varied in colour, which indicated that the PP was covered tightly by the GO based (GOSP/PP-0.1 and GOSP/PP-1) or PVA based (GOSP/PP-10) layer. When the PVA concentration was increasing, the nano-structure of the deposited layer was transformed from 2D laminates to mixed matrix hybrids, in line with the colour change from dark brown to light brown. Derived from these images, the corresponding 3D models were built up as inserted in the images to analyse the surface roughness. As listed in Table 2, the bulk surface roughness was increased from 1.44 μm (PP) to 1.84 μm (GOSP/PP-0.1) after GO/PVA/SSA surface modification. With the increasing of the PVA content, there was an increasing trend in the surface roughness for the GOSP/PP membranes since the increased PVA loading could disorder the regularly packing of the GO nanosheets as evidenced in the XRD results.

To further investigate the microstructure, both surface and cross-sections of the membranes were imaged using SEM as shown in Fig. 6. Compared with the PP with open pores on the surface (Fig. 6a), GOSP/PP membranes revealed the successful deposition of a dense layer on the PP surface (Fig. 6 b-d). Some concave indentations can be found on their surfaces, implying local curving of the flexible GO nanosheets induced by the vacuum pressure during the filtration process. The concave indentations on the membrane surface effectively reduced with increased PVA content from GOSP/PP-1 to GOSP/PP-10, showing a smoother laminating layer in the imaged area. However, it should be noted that tiny pinholes can be observed on the surface of GOSP/PP-0.1 and GOSP/PP-1 in high-resolution images (Fig.S3a-c, SI). This phenomenon could be attributed to the penetration of the coating material into the PP substrate since PVA, SSA and some GO nanosheets were smaller than the surface pore sizes of the PP. To verify this, the cross-sectional SEM

Table 2
Surface roughness of the PP and GOSP/PP membranes.

Membrane	PP	GOSP/PP-0.1	GOSP/PP-1	GOSP/PP-10
Surface roughness (μm)	1.44	1.84	1.95	2.94

imaging was conducted. It can be seen from Fig. 6 (e)-(h) that some pore channels of the PP were blocked due to the intrusion of the coating material. As a result, the GOSP/PP membrane had a dense layer intimately attached on top with partially anchoring structure into the PP pores while keeping the structural stability of the HFs (Fig. S3d). In addition, it was also possible that the increase in the PVA loading could significantly reduce the regularity of the GO alignment from 2D laminar structure to mixed matrix structure while enhancing the intrusion as observed from Fig. 6 (e)-(h).

3.3. Hydrophilic/hydrophobic properties of the membrane surfaces

As shown in the Fig. 7, both the outer and inner surfaces of the PP hollow fibre were hydrophobic by exhibiting WCAs of 118 ± 2°. In contrast, the deposition of the GO/PVA/SSA mixture demonstrated hydrophilic outer surfaces of the GOSP/PP membranes with values of 54.6, 53.3 and 62.6° for GOSP/PP-0.1, GOSP/PP-1 and GOSP/PP-10, respectively. The hydrophilic outer surfaces were due to the presence of hydrophilic groups from GO, PVA and SSA. In addition, the inner surfaces of the GOSP/PP membranes remained hydrophobic by keeping the WCAs in the range of 115–120°, attesting that no GO and/or PVA seeped through to the inner surface during the membrane preparation process. Therefore, the surface modification of the PP HF by the GO/
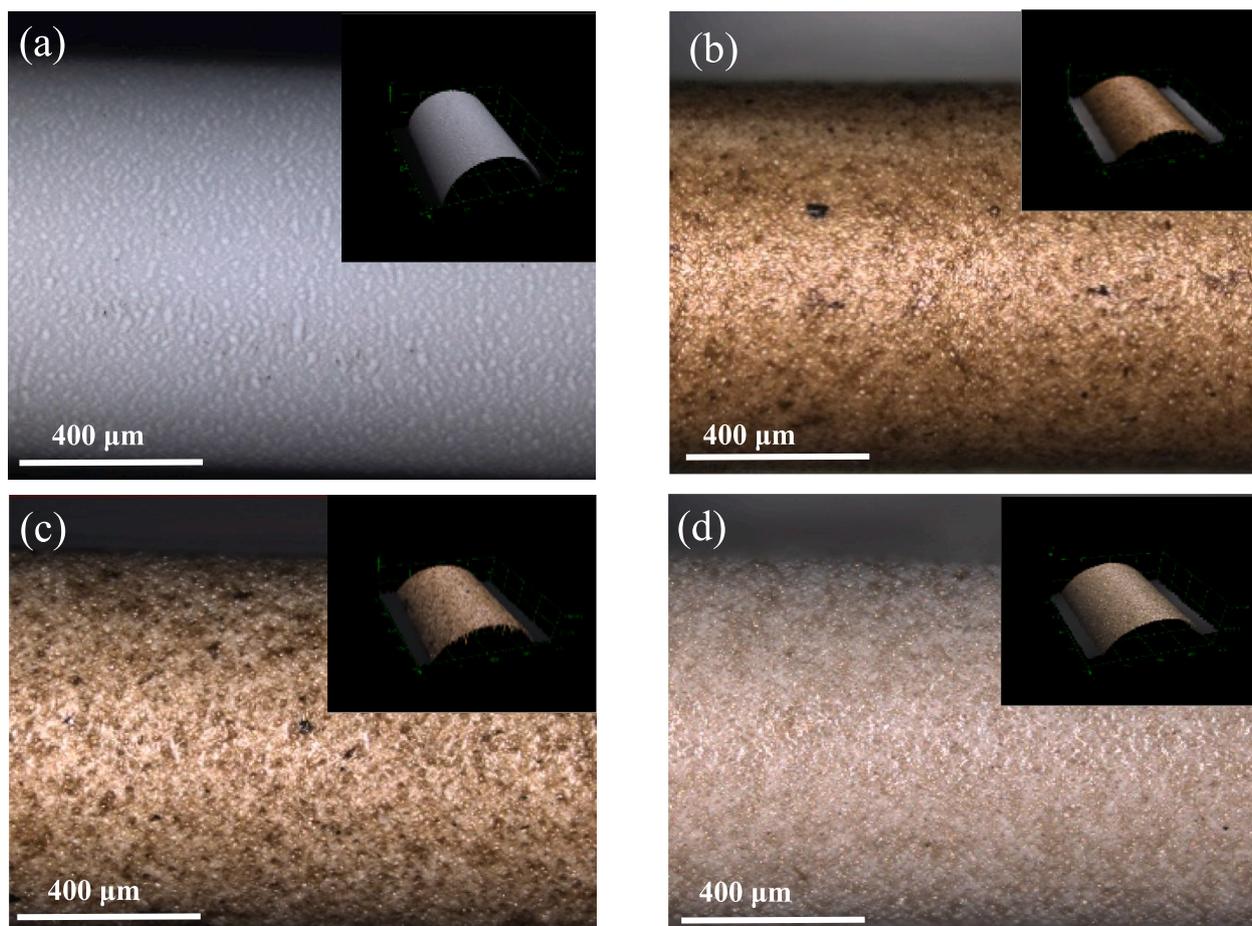
Fig. 5. 3D surface roughness of PP HF and GOSP/PP HF membranes; (a) PP HF, (b) GOSP/PP-0.1, (C) GOSP/PP-1, (d) GOSP/PP-10.
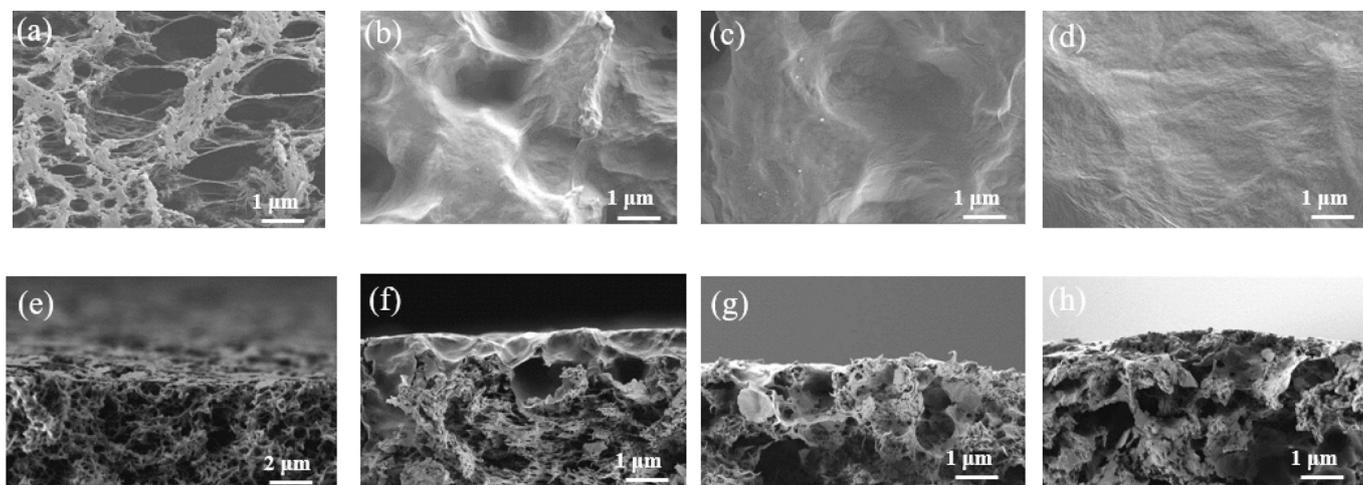
Fig. 6. SEM images of the PP and GOSP/PP membranes; (a) surface view of the PP, (b) surface view of the GOSP/PP-0.1, (c) surface view of the GOSP/PP-1, (d) surface view of the GOSP/PP-10, (e) cross-section view of the PP, (f) cross-section view of the GOSP/PP-0.1, (g) cross-sectional view of the GOSP/PP-1, (g) cross-section view of the GOSP/PP-10.
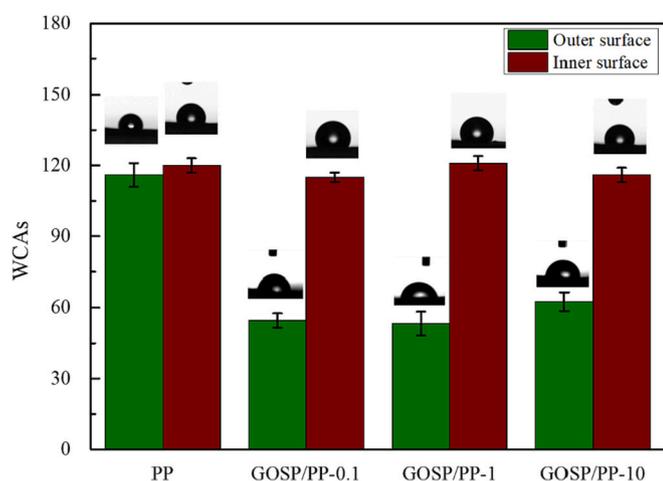
Fig. 7. WCAs of membrane outer and inner surfaces.

PVA/SSA mixture effectively rendered the outer surface hydrophilic while maintaining the hydrophobicity of the inner surface, forming a Janus structured membrane.

3.4. Pore sizes of the Janus membranes

The pore sizes of the fabricated GOSP/PP membranes were measured using capillary flow porometers and the pore size distribution was presented in Fig. 8. For the pristine PP, the mean pore size was 0.41 μm whereas all the GOSP/PP membranes showed reduced pore sizes. To be specific, the GOSP/PP-0.1 membrane had an average pore size of 0.23 μm while the GOSP/PP-1 exhibited two major peaks in the pore size distribution, centering at 0.20 and 0.31 μm, respectively. The sharpest pore size distribution with the majority of the pores allocating at 0.21 μm was observed for the GOSP/PP-10 membrane. This could be contributed to the penetration into the PP layer and pore blockage with the increased PVA concentration. As shown in the SEM images, the vacuum filtration of the GO/PVA/SSA mixture through the PP substrate could effectively form a dense layer atop the PP layer with possible intrusion. As a result, the average pore size of the fabricated GOSP/PP membrane was reduced due to the presence of the GO based or PVA based dense layer. Furthermore, it can also be seen that the increase in the PVA contents was beneficial for the continuous reduction of the pore
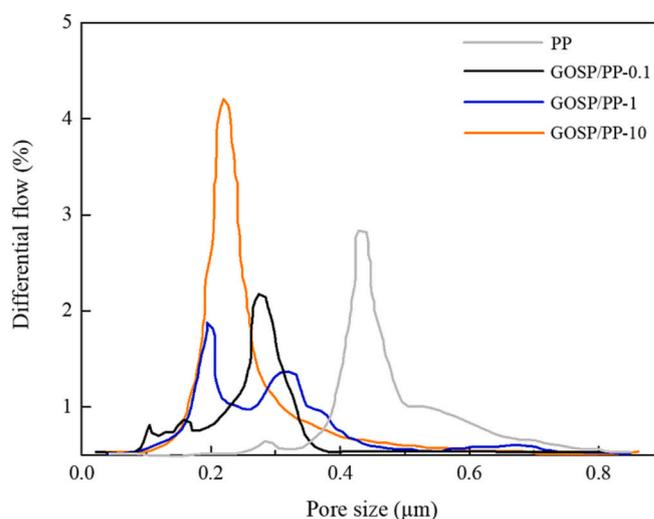
Fig. 8. Pore size results of the membranes.

sizes, suggesting the increased deposition of PVA molecules in the pore channels.

3.5. LEP measurements

LEP is an important characteristic to determine the wettability of the MD membranes and a higher LEP is desired to prevent membrane wetting. Compared with pristine PP that exhibited a LEP of 398 kPa, the GOSP/PP membranes had comparable LEPs of 424 kPa for GOSP/PP-0.1 and 408 kPa for GOSP/PP-1 whereas the GOSP/PP-10 had significantly decreased LEP of 73 kPa (Fig. 9). The obviously lower LEP of GOSP/PP-10 was because the increase in the PVA contents led to greater likelihood of penetrating further into the pores and thus rendered a significant part of the pores as hydrophilic. In this case, the membrane exhibited a hydrophilic-assisted mass transport property and thus the pressure that was required for the liquid to flow through the rest of the pores was much lower. For the GOSP/PP-0.1 and 1 membranes, the intrusion was slight and the increase in the LEP can be resulted from the additional capillary pressure (P_c) derived by the Young−Laplace equation (Eq. (5)) where γ represents the liquid surface tension, θ is the contact angle of the membrane surface, and the d is the average pore diameter [45].
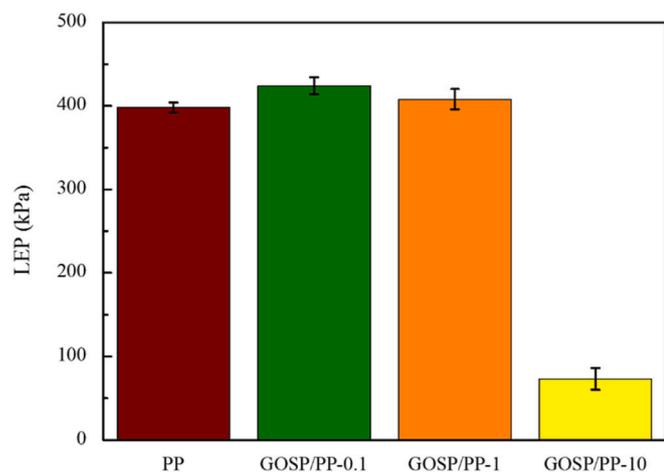
Fig. 9. LEPs of the membranes.

$$P_c = \frac{4\gamma \cos\theta}{d} \qquad (5)$$

It was known that the pore sizes were decreased and the contact angles were <90°. When in contact with the GOSP/PP membrane surfaces, water molecules were firstly drawn into the dense GO/PVA/SSA hydrophilic layer followed by penetrating through to the hydrophobic PP layer, in which the capillary pressure at the GOSP and PP interface could endow resistance for the water transport, imposing extra pressure to the critical transmembrane pressure. In order to further investigate the effect of intrusion on the LEPs, various GO concentrations, i.e., 10, 50 and 100 mg/L with fixed amount of PVA and SSA ratio (same as GOSP/PP-0.1) were measured as a comparison. As shown in Fig.S4 in the SI, the LEPs increased continuously from 399 kPa to 455 kPa when the GO concentration was increased from10 mg/L to 100 mg/L. This suggested that the GO nanosheets were effectively covering the hydrophobic pores and forming a dense hydrophilic layer on top whereas the PVA molecules were apt to infiltrate into the pores.

3.6. DCMD performance of the membranes

Desalination of 3.5 wt% NaCl solution by DCMD was carried out to probe the separation properties of the fabricated membranes. As shown

in Fig. 10, the pristine PP HF membrane exhibited 4.9 ± 0.2 kg/m² h of water vapor flux and 99.8 % of salt rejection whereas the GOSP/PP membranes showed similar salt rejection over 99.5 % with reduced water vapor fluxes that were 3.4 ± 0.2 kg/m² h for the GOSP/PP-0.1, 4.6 ± 0.3 kg/m² h for the GOSP/PP-1 and 4.6 ± 0.3 kg/m² h for the GOSP/PP-10. It is reasonable that the PP had higher water vapor flux considering the reduced pore sizes of the GOSP/PP membranes as evidenced by the pore size distribution data. The GOSP/PP-1 and GOSP/PP-10 exhibited similar water vapor fluxes but they had different mass transport mechanisms (detailed discussion could be found in Section 3.7). To be specific, in the DCMD desalination process, as depicted in Fig. 11, the separation was based on the water vapor diffusion from the liquid-membrane interface down to the permeate side of the membrane. The MD membrane acts as an effective barrier to reject the entry of water while allowing the transport of the vapor under the driving force (partial vapor pressure difference) as occurred in the pristine PP membrane (Fig. 11a). For the GOSP/PP membranes, the presence of the hydrophilic GOSP layer led to the water molecules firstly adsorbing on the surface of the GOSP/PP membranes followed by diffusing towards the interface between the GOSP and PP. The 2D laminar structure of the GOSP-0.1 (Fig. 11b) and GOSP-1 (Fig. 11c) as well as the mixed matrix structure of the GOSP-10 (Fig. 11d) could thereby add resistance for water transport before reaching the permeate side. Meanwhile, due to the partial intrusion, some of the internal pore channels in PP layer could possibly exhibit both hydrophilic and hydrophobic property, i.e., a Janus pore structure as shown in Fig. 11c and d, thereby leading to a reduced distance for vapor transport through the pores. Therefore, for some pores that were penetrated by the casting solution, the GOSP/PP membranes featured the transport behaviours including the permeation through the hydrophilic layers as well as that through the intrusion modified pore channels. For some pores that were not intruded, the transport was realized by water permeation through the hydrophilic layer and the vapor transport through hydrophobic layer. Moreover, it can be seen that the water vapor flux was increased with the augment of PVA concentration, indicating that the mixed matrix structure was beneficial for promoting the water transport through the Janus structure, possibly owing to the boosting of water evaporation through the polymer-based separating layer and the intrusion that reducing the vapor transport path, in line with our previous study [15]. On the other hand, the LEPs of the GOSP/PP membranes were also decreasing with the addition of PVA. It suggested the hydrophobic forces of the GOSP/PP membrane membranes were impaired, which favoured the penetration
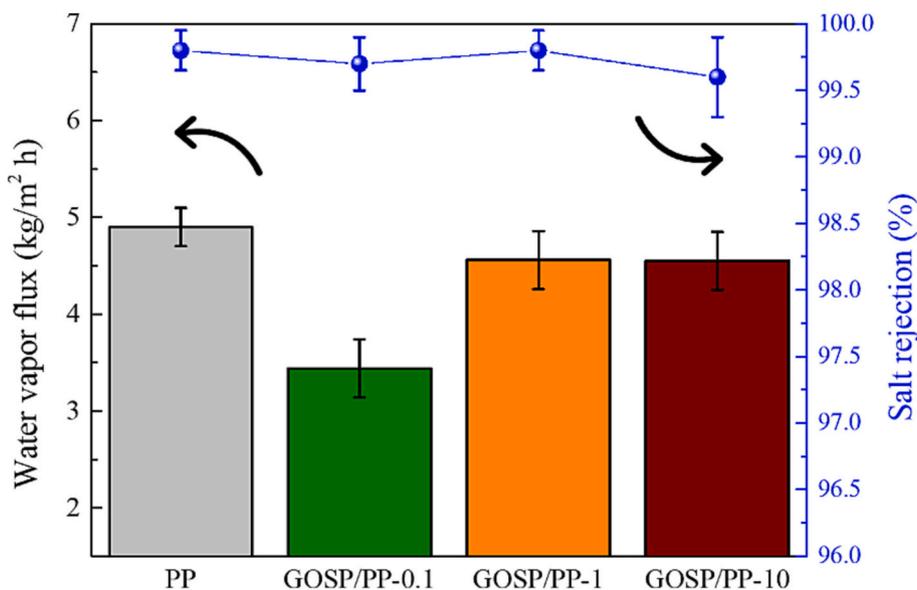
Fig. 10. (a) DCMD performance comparison using 3.5 wt% NaCl solution as the feed; the feed temperature was 50 °C and the permeate temperature was 10 °C.
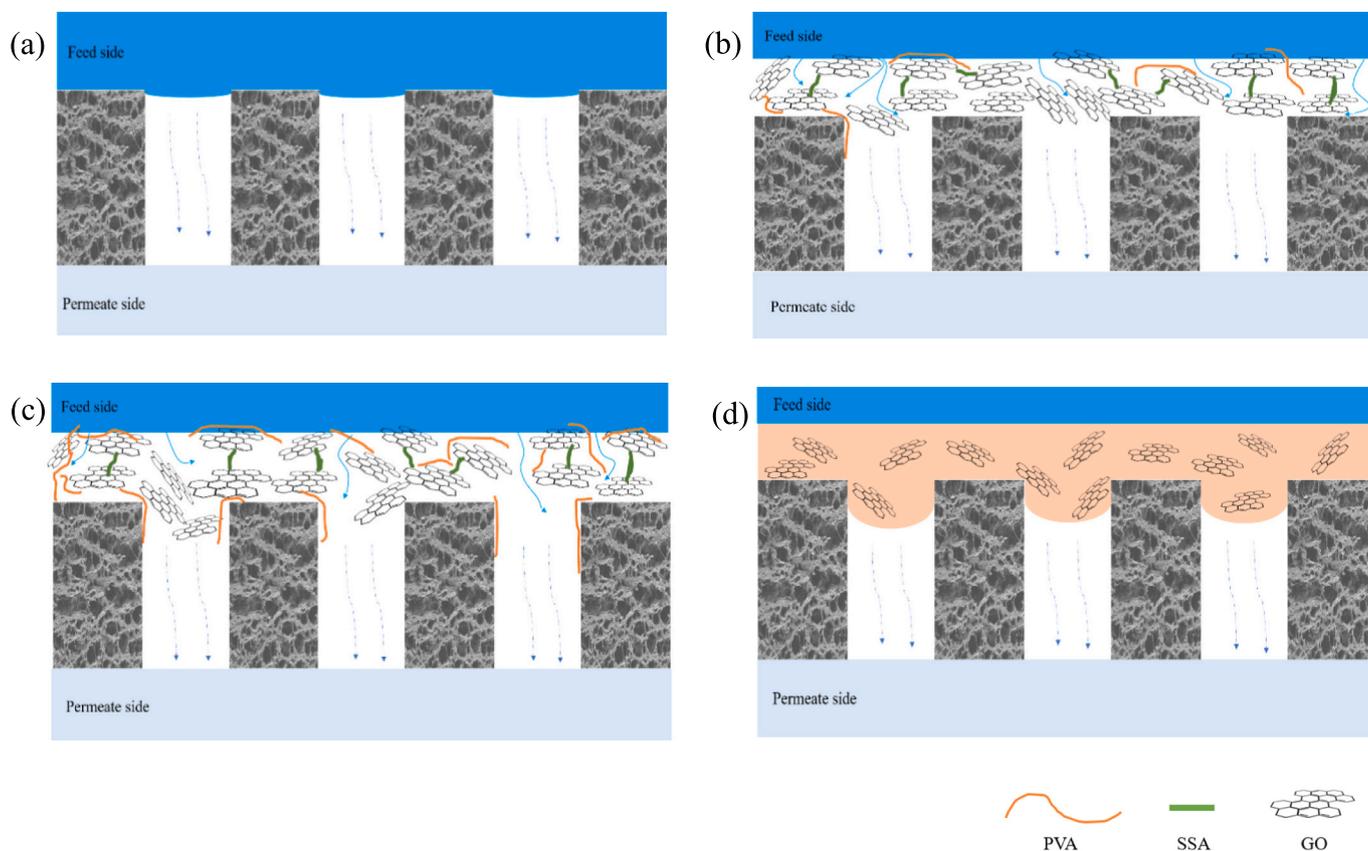
Fig. 11. Transmembrane behaviours in the membranes; (a) pristine PP membrane; (b) GOSP/PP-0.1 membrane; (c) GOSP/PP-1 membrane; (d) GOSP/PP-10 membrane.

of water into the membrane pores [46].

3.7. Antiwetting properties of the fabricated membranes

In order to investigate the antiwetting property of the membranes, pristine PP and the GOSP/PP membranes prepared from various PVA/GO ratio or GO concentrations with fixed PVA ratio, were tested using aqueous mixture containing 3.5 wt% NaCl and 0.4 mM SDS surfactant as the feed solution. In Fig. 12a, the permeate conductivity versus time was drawn to visualize the impact of surfactant on the stability of the membrane during the DCMD process. Compared to the pristine PP membrane, both the GOSP/PP-0.1 and GOSP/PP-1 exhibited superior wetting resistance as evidenced by the time-lag when the emergence of the uptrend in permeate conductivity was observed. Nevertheless, pore wetting occurred to the GOSP/PP-10 membrane earlier than the pristine PP membrane as identified by the substantial increase in salt rejection. This is in consistent with the LEP result that the GOSP/PP-10 had the lowest LEP and thus less wetting resistance. In general, the amphiphilic SDS molecules contribute to the reduction of LEP by reducing the feed surface tension as well as forming hydrophobic-hydrophobic interaction with the membranes, leading to the immobilization of the hydrophilic heads on the internal pore surface. Consequently, a water bridge is
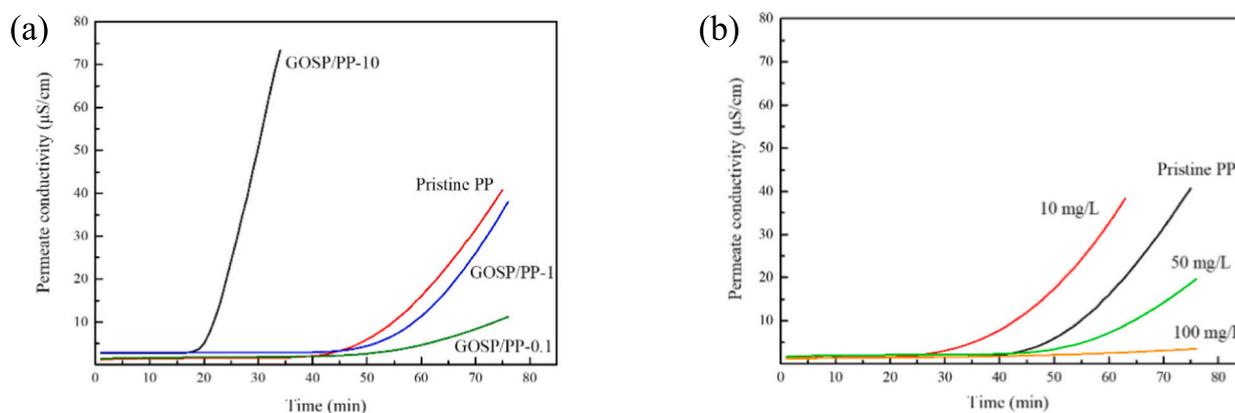
Fig. 12. Antiwetting performance tests: (a) GOSP/PP membranes with various PVA concentrations; (b) GOSP/PP-0.1 membranes with various GO concentrations.

thereby formed and the saline feed solution could infiltrate into the pores, leading to the passage of salts. However, upon the attachment of the GOSP layer, the membrane surface became hydrophilic. Therefore, instead of the hydrophobic-hydrophobic interactions between the surfactant and the PP, the existence of the hydrophilic layer intended to form attractive interactions with the hydrophilic head while repelling the hydrophobic tail. As such, formation of the water bridge by surfactant could be effectively avoided. The enhanced wetting resistance for the GOSP/PP-0.1 and GOSP/PP-1 was also well aligned with the increased LEP values. However, it can be identified that the increase in the PVA loading was detrimental for antiwetting behavior of the GOSP/ PP membranes, particularly as the GOSP/PP-10 membrane exhibited declined wetting resistance. It was demonstrated in the cross-section view that PVA leaded to severe intrusion of the GOSP layer when its content was 10 times that of the GO. That was mainly due to the penetration of PVA molecules and their attachment on the internal pore surface as depicted in Fig. 11d. On the other hand, it can be seen from the WCA results that no hydrophilic materials penetrated through to the downstream side of the PP membrane since the inner surface of the PP membrane remained hydrophobic. Therefore, the intrusion was partial in the pores, leading to the PP pore channels with both hydrophilic and hydrophobic parts, i.e., a Janus transport path through the pores. In this case, the hydroxy groups from PVA provided the "water bridge" partially, resulting in the pores more easily to be wetted. When the PVA amount was low, the intrusion in the pores was not supposed to be as deep as that of high PVA concentration (10 times of the GO). The PVA molecules mainly functioned as the spacer to modify the GO with possible covalent linkages as evidenced in the FTIR results, which enhanced the structural stability of the 2D GO based layer.

Apart from the impact of PVA, the amount of GO deposited on the PP was further investigated by changing the GO concentration in the aqueous mixture. As shown in Fig. 12b, the antiwetting capability corresponded well with the GO concentration, that is, the membrane prepared from the solution containing 100 mg/L GO exhibited the least tendency in the increase of the permeate conductivity whereas those prepared from 10 mg/L and 50 mg/L GO solutions (10 % PVA and 20 % SSA) was unable to sustain the salt rejection after 40 min and showed greater gradient in the increase of permeate conductivity. These results indicated that with only 10 or 50 mg/L GO in the solution, the reduced effective pore sizes of the GOSP/PP membranes with the pinholes were not able to prevent the pores from the surfactants in the feed. The wetting of the membrane pores was alleviated but still not completely prohibited. When the GO concentration increased to 100 mg/L, the effective pore size of the GOSP/PP membrane was further reduced by covering the pinholes since there were enough deposited GO nanosheets. As a result, the GOSP layer became denser and thicker, and was beneficial for avoiding the contact between the surfactants and PP.

3.8. Antifouling properties and long-term stability of the fabricated membranes

To further demonstrate the fouling resistance improvement for the modified membrane, GOSP/PP-0.1(100) and pristine PP membranes were subjected to DCMD desalination with the addition of mineral oil over time into the feed solution as shown in Fig. 13. Initially, with the first 2 additions of 110 mg mineral, both PP and GOSP/PP-0.1(100) showed no decline of flux. But after passing 210 min mark with a cumulative addition of 940 mg mineral oil, the PP membrane started to exhibit sudden drop in flux with close to 10 % reduction and severe inconsistency in flux was observed. This was because of the interactions between the oil and PP membrane, that is, non-polar oils can easily adhere to pristine PP membrane by hydrophobic interactions. For the GOSP/PP-0.1(100) membrane, on the other hand, it did not encounter such sudden flux drop. However, it started to show signs of gradual flux decrease with time. At 470 min mark, another 500 mg of mineral oil was added into the feed solution, the PP membrane exhibited continuous
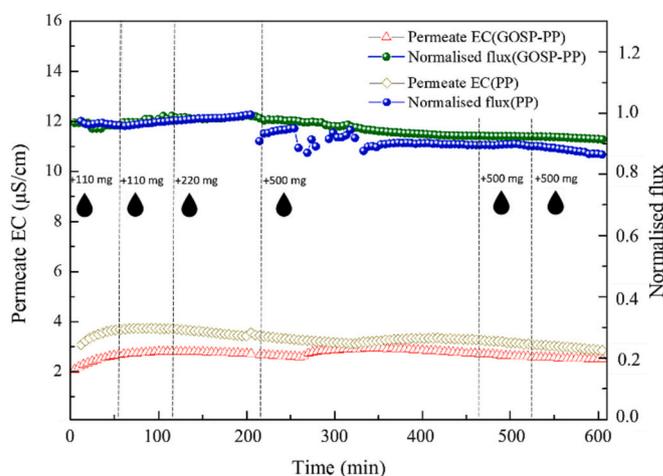
Fig. 13. Normalized water flux and permeate EC of control and GOSP/PP-0.1 (100) measured in DCMD using 3.5 % NaCl and sequential addition of mineral oil at 60 °C as feed solution and DI water at 10 °C as permeate solution.

drop in the flux while the flux of the GOSP/PP-0.1(100) was stable. After over 520 min of the DCMD run, the control membrane had a flux drop of around 15 % whereas GOSP/PP-0.1(100) retained its flux performance. Both PP and GOSP/PP-0.1(100) showed no obvious sign of membrane wetting throughout the test, indicating that mineral oil only acted as foulant but not wetting agent. The permeate EC was stable throughout the DCMD tests, in the range of 0.18–0.3 μS/cm for which the GOSP/PP-0.1(100) exhibited relatively lower EC, indicating better membrane selectivity.

To evaluate the long-term stability of the GOSP/PP-0.1(100) membrane for practical application, desalination of real seawater was conducted using the seawater collected from Black Rock (Melbourne, Australia). As shown in Fig. 14a, the permeate EC was stable around 2.1–2.9 μS/cm when the DCMD test was ended at 75 % water recovery. The water vapor flux remained steady (4.6 kg/m² h) during the operation of 75 h. Furthermore, real leachate was used as the feed to evaluate the wetting and fouling property since leachate contains complex fouling and wetting inducing organic compounds. As expected, no fouling or wetting phenomenon was evident for the GOSP/PP-0.1(100) since the membrane exhibited stable salt rejection of over 99.9 % and water vapor flux of 4.7 kg/m² h until the test ended at 80 % water recovery. Such stable separation performance of this Janus membrane towards both seawater desalination and leachate concentration was mainly due to the anchoring of the GOSP layer that was constructed via the covalent linkages between the GO, PVA and SSA. As evidenced by the SEM, XRD, 3D laser microscope and WCA measurements, the anchored structure of the Janus membrane ensured membrane integrity against long-term immersion in the aqueous environment and hydrophilicity of the GOSP layer could effectively mitigate the membrane fouling by avoiding the hydrophobic interactions between the membrane and foulants. The robust performance of the GOSP/PP-0.1(100) membrane for leachate treatment could also be reflected in the photos as shown in Fig. 15. After the DCMD process, the brown leachate feed solution with an initial American Dye Manufacturers Institute (ADMI) colour unit of 2672 was concentrated by ~9 times to 22,932 colour units. While the permeate remained clear (<10 colour unit). Furthermore, permeate ion concentration and organic matter concentration was provided by ICP-OES and chemical oxygen demand (COD) measurements (Table S2 in the SI). It can be seen that almost all impurities were enriched in the post-run feed solution and high quality permeate was produced with <1 mg/L of ions and 10 mg/L of organics. After the long-term test, membrane cleaning was undertaken using tap water as the cleaning agent. By simply tap water washing, the GOSP/PP-0.1(100) exhibited 100 % of the initial water flux as well as salt rejection when
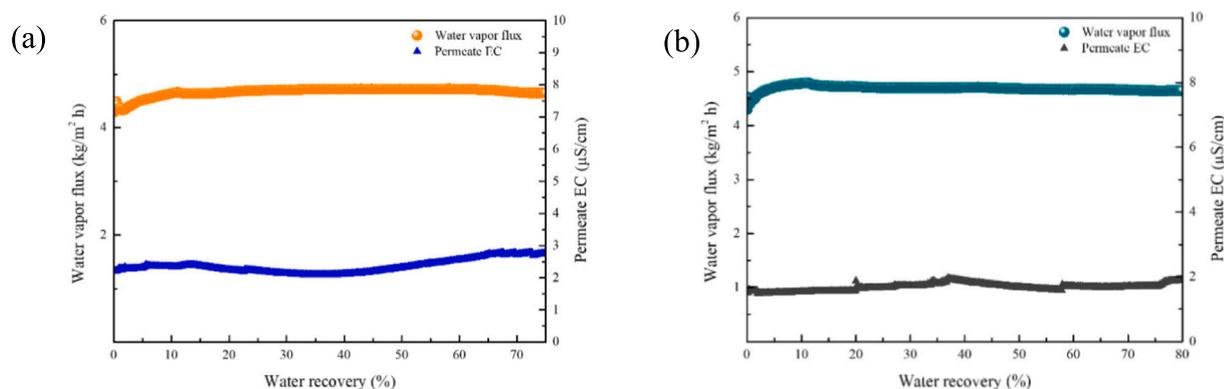
Fig. 14. Water vapor flux and permeate EC of GOSP/PP-0.1(100) measured in DCMD using real seawater (a) and industrial leachate (b), respectively, at 60 °C as feed solution and DI water at 10 °C as permeate solution.

Fig. 15. Pictures of the leachate as received (left); feed concentrate after MD treatment (middle); and permeate (right).

reprocessing the leachate. The leachate DCMD test following the membrane cleaning was conducted for 5 h and repeated for 3 times. The membrane cleaning effectiveness was listed in Table S3 in the SI. It can be seen that after 3 repeats, 100 % of the initial separation performance could be obtained, proving the outstanding stability of the fabricated Janus membrane.

As shown in Table 3, the antiwetting and antifouling performances of the reported Janus membranes prepared with various materials were compared. It can be seen that the GOSP/PP-0.1(100) membrane exhibited better stability than most of the flat sheet membranes while the other HF membranes composed of polydopamine, polyethylene glycol, sodium periodate, PVDF, etc., were capable of processing synthetic oil-in-water emulsion for over 96 h. However, the GOSP/PP-0.1 (100) was subjected to leachate without pretreatment and exhibited no decline in the separation performance after tap water cleaning. These results demonstrate the potential applicability of using GOSP based

Table 3
Comparison of the reported hydrophilic/hydrophobic membranes in antiwetting and antifouling performances during MD operation.

Membrane type	Membrane materials	Configuration	Feed/permeate temperature (°C)	Feed composition	Performance without fouling or wetting (h)	Ref
Flat sheet	GO/PVDF	DCMD	65/20	50 mg/L sodium dodecyl benzene sulfonate solution	5	[47]
Flat sheet	Polyurethane/PTFE	DCMD	50/10	40 mg/L SDS solution	90	[16]
Flat sheet	Polydopamine/PTFE	vacuum MD	60/−	500 mg/L mineral oil	40	[48]
Flat sheet	Agarose/PTFE	DCMD	60/20	10 mg/L Tween® 20 and 500 mg/L SDS	24	[49]
Flat sheet	Polydopamine/SiNP/PVDF	DCMD	60/20	1000 mg/L oil-in-water emulsion	12	[50]
Flat sheet	Glutaraldehyde/PVA/PTFE	DCMD	53/20	1000 mg/L oil-in-water emulsion	30	[51]
Flat sheet	Polyethylene glycol/TiO$_2$/PVDF	DCMD	60/20	0.01 wt% oil-in-water emulsion	24	[52]
HF	Polydopamine/ Polyethylene glycol/PVDF	DCMD	60/20	500 mg/L oil-in-water emulsion	168	[53]
HF	Polydopamine/sodium periodate/PVDF	DCMD	60/20	500 mg/L oil-in-water emulsion	140	[54]
HF	Polydopamine/sodium periodate/Ag/PVDF	DCMD	60/20	500 mg/L oil-in-water emulsion	96	[21]
HF	GOSP/PP-0.1(100)	DCMD	50/20	Leachate	80	This work

Janus membrane in MD process for leachate concentration and high water recovery, which are highly desirable for practical wastewater treatment with a focus on zero liquid discharge.

4. Conclusion

In summary, Janus hollow fibre membrane with an internally covalent-linked hydrophilic GOSP layer on top of a microporous hydrophobic PP support layer was formed through an ethanol-assisted vacuum filtration process for DCMD applications. The GOSP hydrophilic layer featured partial intrusion into the pore channels of the PP, leading to a tightly anchored Janus structure with hydrophilic surface and thus a Janus pore structure. The interlayer spacing of the GOSP membrane was enlarged due to the intercalation of PVA while the swelling of the GO laminates was effectively restrained via the linkage between GO, PVA and SSA. However, at the higher PVA/GO ratio as in GOSP/PP-10, the structure of the GOSP was altered from 2D laminar membrane to mixed matrix membrane accompanied with abundant intrusion into the PP pore channels. This resulted in reduction of the LEP while the attachment of the GO based GOSP layer (GOSP-0.1 and GOSP-1) increased the LEP of the GOSP/PP membrane. With rational manipulation of the hydrophilic layer, the GOSP/PP-0.1 membrane exhibited stable water flux, high salt rejection and enhanced anti-wetting property towards surfactant SDS containing feed solution. The stability of the GOSP/PP-0.1 membrane was further examined for real seawater desalination and leachate treatment. Stable water vapor fluxes and high salt rejections were maintained throughout the DCMD process. Even at high water recovery (~80 %) and 5 times leachate concentration, the GOSP/PP-0.1 membrane still exhibited superior robustness and wetting resistance, demonstrating the great potential for practical application of MD for wastewater treatment towards zero liquid discharge.

CRediT authorship contribution statement

Guang Yang: Formal analysis, Validation, Writing – original draft. **Derrick Ng:** Methodology, Formal analysis, Writing – review & editing. **Zhen Huang:** Investigation, Methodology, Validation. **Jianhua Zhang:** Validation, Writing – review & editing. **Stephen Gray:** Writing – review & editing. **Zongli Xie:** Conceptualization, Supervision, Writing – review & editing, Project administration.

Declaration of competing interest

The authors declare that they have no known competing financial interests or personal relationships that could have appeared to influence the work reported in this paper.

Data availability

Data will be made available on request.

Appendix A. Supplementary data

Supplementary data to this article can be found online at https://doi.org/10.1016/j.desal.2023.116423.

References

[1] J.S. Baker, L.Y. Dudley, Biofouling in membrane systems — a review, Desalination 118 (1998) 81–89.
[2] R. Semiat, Energy issues in desalination processes, Environ. Sci. Technol. 42 (2008) 8193–8201.
[3] H. Zhao, S. Qiu, L. Wu, L. Zhang, H. Chen, C. Gao, Improving the performance of polyamide reverse osmosis membrane by incorporation of modified multi-walled carbon nanotubes, J. Membr. Sci. 450 (2014) 249–256.
[4] A. Alkhudhiri, N. Darwish, N. Hilal, Membrane distillation: a comprehensive review, Desalination 287 (2012) 2–18.
[5] E. Drioli, A. Ali, F. Macedonio, Membrane distillation: recent developments and perspectives, Desalination 356 (2015) 56–84.
[6] J. Ravi, M.H.D. Othman, T. Matsuura, M. Ro'il Bilad, T.H. El-badawy, F. Aziz, A. F. Ismail, M.A. Rahman, J. Jaafar, Polymeric membranes for desalination using membrane distillation: a review, Desalination 490 (2020), 114530.
[7] J. Ge, Y. Peng, Z. Li, P. Chen, S. Wang, Membrane fouling and wetting in a DCMD process for RO brine concentration, Desalination 344 (2014) 97–107.
[8] X. An, Z. Liu, Y. Hu, Amphiphobic surface modification of electrospun nanofibrous membranes for anti-wetting performance in membrane distillation, Desalination 432 (2018) 23–31.
[9] D. Hou, C. Ding, C. Fu, D. Wang, C. Zhao, J. Wang, Electrospun nanofibrous omniphobic membrane for anti-surfactant-wetting membrane distillation desalination, Desalination 468 (2019), 114068.
[10] L.D. Tijing, Y.C. Woo, J.-S. Choi, S. Lee, S.-H. Kim, H.K. Shon, Fouling and its control in membrane distillation—a review, J. Membr. Sci. 475 (2015) 215–244.
[11] Z. Wang, Y. Chen, X. Sun, R. Duddu, S. Lin, Mechanism of pore wetting in membrane distillation with alcohol vs. surfactant, J. Membr. Sci. 559 (2018) 183–195.
[12] N.M. Mokhtar, W.J. Lau, A.F. Ismail, The potential of membrane distillation in recovering water from hot dyeing solution, <sb:contribution><sb:title>J. Water</sb:title></sb:contribution><sb:host><sb:issue><sb:series><sb:title>Process. Eng.</sb:title></sb:series></sb:issue></sb:host> 2 (2014) 71–78.
[13] W. Wang, X. Du, H. Vahabi, S. Zhao, Y. Yin, A.K. Kota, T. Tong, Trade-off in membrane distillation with monolithic omniphobic membranes, Nat. Commun. 10 (1) (2019) 3220.
[14] G. Yang, J. Zhang, M. Peng, E. Du, Y. Wang, G. Shan, L. Ling, H. Ding, S. Gray, Z. Xie, A mini review on antiwetting studies in membrane distillation for textile wastewater treatment, Processes 9 (2) (2021) 243.
[15] Z. Huang, G. Yang, J. Zhang, S. Gray, Z. Xie, Janus membranes with a thin film hydrophilic MOF/PVA nanocomposite for enhanced antiwetting property in membrane distillation, Desalination 518 (2021).
[16] D. Cheng, J. Zhang, N. Li, D. Ng, S.R. Gray, Z. Xie, Antiwettability and performance stability of a composite hydrophobic/hydrophilic Janus membrane in wastewater treatment by membrane distillation, Ind. Eng. Chem. Res. 57 (28) (2018) 9313–9322.
[17] S. Bonyadi, T.S. Chung, Flux enhancement in membrane distillation by fabrication of dual layer hydrophilic–hydrophobic hollow fiber membranes, J. Membr. Sci. 306 (1–2) (2007) 134–146.
[18] H. Song, H. Yu, L. Zhu, L. Xue, D. Wu, H. Chen, Durable hydrophilic surface modification for PTFE hollow fiber membranes, React. Funct. Polym. 114 (2017) 110–117.
[19] M. Afsari, H.K. Shon, L.D. Tijing, Janus membranes for membrane distillation: recent advances and challenges, Adv. Colloid Interf. Sci. 289 (2021), 102362.
[20] Y.X. Huang, Z. Wang, J. Jin, S. Lin, Novel janus membrane for membrane distillation with simultaneous fouling and wetting resistance, Environ Sci Technol 51 (22) (2017) 13304–13310.
[21] N.G.P. Chew, Y. Zhang, K. Goh, J.S. Ho, R. Xu, R. Wang, Hierarchically structured janus membrane surfaces for enhanced membrane distillation performance, ACS Appl. Mater. Interfaces 11 (28) (2019) 25524–25534.
[22] N.G.P. Chew, S. Zhao, R. Wang, Recent advances in membrane development for treating surfactant- and oil-containing feed streams via membrane distillation, Adv. Colloid Interf. Sci. 273 (2019), 102022.
[23] H.C. Yang, J. Hou, V. Chen, Z.K. Xu, Janus membranes: exploring duality for advanced separation, Angew. Chem. Int. Ed. Engl. 55 (43) (2016) 13398–13407.
[24] Q.-C. Xia, M.-L. Liu, X.-L. Cao, Y. Wang, W. Xing, S.-P. Sun, Structure design and applications of Janus polymeric membranes, J. Membr. Sci. 562 (2018) 85–111.
[25] Z.-Y. Wang, Z.-J. Fu, D.-D. Shao, M.-J. Lu, Q.-C. Xia, H.-F. Xiao, B.-W. Su, S.-P. Sun, Bridging the miscibility gap to fabricate delamination-free Janus nanofiltration membranes via incorporating fluoro substituted aromatic amine, J. Membr. Sci. 610 (2020).
[26] M. Wang, J.S. Oh, N.T. Mai, S. Kim, S. Hong, T. Hwang, Y. Lee, J.D. Nam, D. Duong le, Large-area, conductive and flexible reduced graphene oxide (RGO) membrane fabricated by electrophoretic deposition (EPD), ACS Appl. Mater. Interfaces 6 (3) (2014) 1747–1753.
[27] K. Huang, G. Liu, Y. Lou, Z. Dong, J. Shen, W. Jin, A graphene oxide membrane with highly selective molecular separation of aqueous organic solution, Angew. Chem. Int. Ed. Engl. 53 (27) (2014) 6929–6932.
[28] J.Y. Chong, B. Wang, K. Li, Water transport through graphene oxide membranes: the roles of driving forces, Chem. Commun. 54 (20) (2018) 2554–2557.
[29] S. Dervin, D.D. Dionysiou, S.C. Pillai, 2D nanostructures for water purification: graphene and beyond, Nanoscale 8 (33) (2016) 15115–15131.
[30] M. Bhadra, S. Roy, S. Mitra, Desalination across a graphene oxide membrane via direct contact membrane distillation, Desalination 378 (2016) 37–43.

[31] S. Valizadeh, L. Naji, M. Karimi, Controlling interlayer spacing of graphene oxide membrane in aqueous media using a biocompatible heterobifunctional crosslinker for penicillin-G procaine removal, Sep. Purif. Technol. 263 (2021).

[32] S. Kim, R. Ou, Y. Hu, X. Li, H. Zhang, G.P. Simon, H. Wang, Non-swelling graphene oxide-polymer nanocomposite membrane for reverse osmosis desalination, J. Membr. Sci. 562 (2018) 47–55.

[33] G. Yang, Z. Xie, M. Cran, D. Ng, C.D. Easton, M. Ding, H. Xu, S. Gray, Functionalizing graphene oxide framework membranes with sulfonic acid groups for superior aqueous mixture separation, J. Mater. Chem. A 7 (34) (2019) 19682–19690.

[34] L. Zou, P. Gusnawan, G. Zhang, J. Yu, Novel Janus composite hollow fiber membrane-based direct contact membrane distillation (DCMD) process for produced water desalination, J. Membr.Sci. 597 (2020).

[35] S.W. Zha, P. Gusnawan, J.J. Lin, G.Y. Zhang, N. Liu, J.J. Yu, Integrating a novel TS-af-HFM NF process for portable treatment of oilfield produced water, Chem. Eng. J. 311 (2017) 203–208.

[36] L.H. Zhao, C.R. Wu, X.L. Lu, D. Ng, Y.B. Truong, Z.L. Xie, Activated carbon enhanced hydrophobic/hydrophilic Janus nanofiber composite membranes for high-performance direct contact membrane distillation, Desalination 446 (2018) 59–69.

[37] C. Boo, J. Lee, M. Elimelech, Engineering surface energy and nanostructure of microporous films for expanded membrane distillation applications, Environ. Sci. Technol. 50 (15) (2016) 8112–8119.

[38] Y. Chen, M. Tian, X. Li, Y. Wang, A.K. An, J. Fang, T. He, Anti-wetting behavior of negatively charged superhydrophobic PVDF membranes in direct contact membrane distillation of emulsified wastewaters, J. Membr. Sci. 535 (2017) 230–238.

[39] M. Khayet, T. Matsuura, Preparation and characterization of polyvinylidene fluoride membranes for membrane distillation, Ind. Eng. Chem. Res. 40 (24) (2001) 5710–5718.

[40] G. Racz, S. Kerker, Z. Kovacs, G. Vatai, M. Ebrahimi, P. Czermak, Theoretical and experimental approaches of liquid entry pressure determination in membrane distillation processes, Period Polytech.-Chem. 58 (2) (2014) 81–91.

[41] S. Pei, H.-M. Cheng, The reduction of graphene oxide, Carbon 50 (9) (2012) 3210–3228.

[42] B. Wang, Z. Chen, J. Zhang, J. Cao, S. Wang, Q. Tian, M. Gao, Q. Xu, Fabrication of PVA/graphene oxide/TiO2 composite nanofibers through electrospinning and interface sol–gel reaction: effect of graphene oxide on PVA nanofibers and growth of TiO2, Colloids Surf. Physicochem. Eng. Aspects 457 (2014) 318–325.

[43] M.M. Aboelhassan, A.F. Peixoto, C. Freire, Sulfonic acid functionalized silica nanoparticles as catalysts for the esterification of linoleic acid, New J. Chem. 41 (9) (2017) 3595–3605.

[44] W.W. Mar, E. Somsook, Sulfonic-functionalized carbon catalyst for esterification of high free fatty acid, Procedia Eng. 32 (2012) 212–218.

[45] Y. Liang, S. Kim, P. Kallem, H. Choi, Capillary effect in Janus electrospun nanofiber membrane for oil/water emulsion separation, Chemosphere 221 (2019) 479–485.

[46] P. Yazgan-Birgi, M.I.Hassan Ali, H.A. Arafat, Estimation of liquid entry pressure in hydrophobic membranes using CFD tools, J. Membr. Sci. 552 (2018) 68–76.

[47] H. Qiu, Y. Peng, L. Ge, B. Villacorta Hernandez, Z. Zhu, Pore channel surface modification for enhancing anti-fouling membrane distillation, Appl. Surf. Sci. 443 (2018) 217–226.

[48] W. Sun, F. Shen, Z. Wang, Y. Zhang, Y. Wan, An ultrathin, porous and in-air hydrophilic/underwater oleophobic coating simultaneously increasing the flux and antifouling property of membrane for membrane distillation, Desalination 445 (2018) 40–50.

[49] P.-J. Lin, M.-C. Yang, Y.-L. Li, J.-H. Chen, Prevention of surfactant wetting with agarose hydrogel layer for direct contact membrane distillation used in dyeing wastewater treatment, J. Membr. Sci. 475 (2015) 511–520.

[50] Z. Wang, J. Jin, D. Hou, S. Lin, Tailoring surface charge and wetting property for robust oil-fouling mitigation in membrane distillation, J. Membr. Sci. 516 (2016) 113–122.

[51] K. Wang, D. Hou, J. Wang, Z. Wang, B. Tian, P. Liang, Hydrophilic surface coating on hydrophobic PTFE membrane for robust anti-oil-fouling membrane distillation, Appl. Surf. Sci. 450 (2018) 57–65.

[52] G. Zuo, R. Wang, Novel membrane surface modification to enhance anti-oil fouling property for membrane distillation application, J. Membr. Sci. 447 (2013) 26–35.

[53] N.G.P. Chew, S. Zhao, C. Malde, R. Wang, Superoleophobic surface modification for robust membrane distillation performance, J. Membr. Sci. 541 (2017) 162–173.

[54] N.G.P. Chew, S. Zhao, C. Malde, R. Wang, Polyvinylidene fluoride membrane modification via oxidant-induced dopamine polymerization for sustainable direct-contact membrane distillation, J. Membr. Sci. 563 (2018) 31–42.